Detecting continuous gravitational waves with superfluid ^{4}He

2017 New J. Phys. 19 073023

(http://iopscience.iop.org/1367-2630/19/7/073023)

New Journal of Physics
The open access journal at the forefront of physics

Deutsche Physikalische Gesellschaft DPG
IOP Institute of Physics

Published in partnership with: Deutsche Physikalische Gesellschaft and the Institute of Physics

OPEN ACCESS

RECEIVED
1 February 2017

REVISED
21 April 2017

ACCEPTED FOR PUBLICATION
12 June 2017

PUBLISHED
21 July 2017

PAPER

Detecting continuous gravitational waves with superfluid ^{4}He

S Singh[1,2,5,6], L A De Lorenzo[3], I Pikovski[2,4] and K C Schwab[3]

[1] Department of Physics, College of Optical Sciences and B2 Institute, University of Arizona, Tucson, AZ 85721, United States of America
[2] ITAMP, Harvard-Smithsonian Center for Astrophysics, Cambridge, MA 02138, United States of America
[3] Applied Physics, California Institute of Technology, Pasadena, CA 91125 United States of America
[4] Department of Physics, Harvard University, Cambridge, MA 02138, United States of America
[5] Present address: Department of Physics, Williams College, Williamstown, MA 01267, United States of America.
[6] Author to whom any correspondence should be addressed.

E-mail: swati.singh@williams.edu **and** schwab@caltech.edu

Keywords: gravitational waves, optomechanics, superfluid helium

Abstract

Direct detection of gravitational waves is opening a new window onto our universe. Here, we study the sensitivity to continuous-wave strain fields of a kg-scale optomechanical system formed by the acoustic motion of superfluid helium-4 parametrically coupled to a superconducting microwave cavity. This narrowband detection scheme can operate at very high Q-factors, while the resonant frequency is tunable through pressurization of the helium in the 0.1–1.5 kHz range. The detector can therefore be tuned to a variety of astrophysical sources and can remain sensitive to a particular source over a long period of time. For thermal noise limited sensitivity, we find that strain fields on the order of $h \sim 10^{-23}/\sqrt{\text{Hz}}$ are detectable. Measuring such strains is possible by implementing state of the art microwave transducer technology. We show that the proposed system can compete with interferometric detectors and potentially surpass the gravitational strain limits set by them for certain pulsar sources within a few months of integration time.

1. Introduction

The recent detection of gravitational waves (GWs) marks the beginning of GW astronomy [1, 2]. The first direct detection confirmed the existence of GWs emitted from a relativistic inspiral and merger of two large black holes (BHs), at a distance of 400M parsecs (pc) [1]. Indirect evidence for gravitational radiation was previously attained by the careful observation since 1974 of the decay of the orbit of the neutron star (NS) binary system PSR B1913+16 at a distance of 6.4 kpc, which agrees with the predictions from general relativity to better than 1% [3]. In this paper, we discuss the potential to use a novel superfluid-based optomechanical system as a tunable detector of narrow-band GWs, which is well suited for probing GWs from nearby pulsars As we discuss below, in the frequency range exceeding ~500 Hz, this novel scheme has the potential to reach sensitivities comparable to Advanced LIGO.

The GW detector under consideration is formed by high-Q acoustic modes of superfluid helium parametrically coupled to a microwave cavity mode in order to detect small elastic strains. This setup was initially studied in [4], and is shown in figure 1. The helium detector effectively acts as a Weber bar antenna [5] for GWs, but with two important differences. Firstly, the Q/T-factor of the helium is expected to be much larger than that of metals, where Q is the acoustic quality factor, and T is the mode temperature. Secondly, the acoustic resonance frequency can be changed by up to 50% by pressurization of helium without affecting the damping rate, making the detector both narrowband and tunable. Recent laboratory experiments [6] have realized quality factors of $Q_{\text{He}} = 1.4 \times 10^8$ for superfluid ^{4}He, which appears to be limited by a combination of ^{3}He impurities, sample temperature, and radiation loss. All of these dissipation mechanisms can be reduced and we assume quality factors of 10^{11} are possible in future experiments with isotropically pure samples at lower temperatures of around 10 mK.

The power spectrum of GWs is expected to be extremely broad and is estimated to range from 10^{-16} to 10^3 Hz [7–9] for known sources. Ground-based optical interferometers (such as LIGO, Virgo, GEO, TAMA) allow

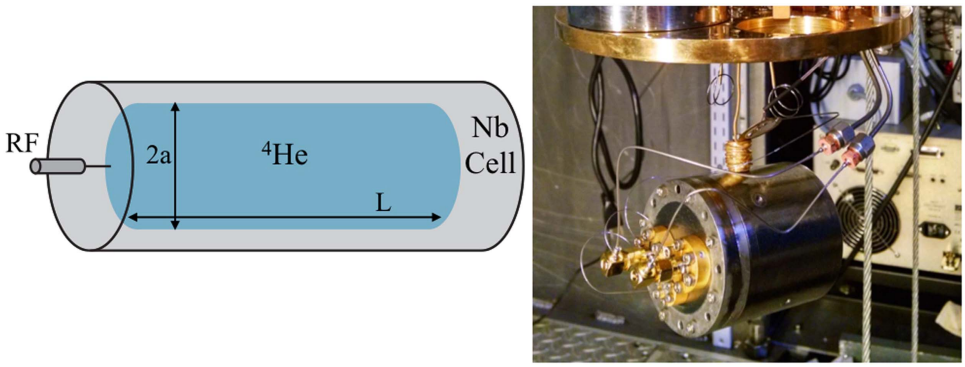

Figure 1. *Left*: schematic of the proposed GW sensor based on acoustic modes of superfluid helium. Two cylindrical geometries considered here are Gen1 (radius $a = 11$ cm, length $L = 50$ cm, mass $M = 2.7$ kg) and Gen2 ($a = 11$ cm, $L = 3$ m, $M = 16$ kg). *Right*: prototype of the detector with $a = 1.8$ cm, $L = 4$ cm, $M = 6$ g and resonant frequency 10 kHz.

for broad-band search for GWs in the frequency range 10 Hz–5 kHz. These detectors are expected to be predominantly sensitive to the chirped, transient, GW impulse resulting from the last moments of coalescing binaries involving compact objects (BHs and/or NSs) [10]. Space-based interferometric detectors can be sensitive to lower frequency GWs, as they are not limited by seismic noise [11].

Unlike broadband impulse sources, rapidly rotating compact objects such as pulsars are expected to generate highly coherent, continuous GW signals due to the off-axis rotating mass, with frequencies spanning from ~1 kHz for millisecond pulsars (MSPs) in binaries, to 1 Hz for very old pulsars [7, 12–15]. Given the unknown mass distribution of the pulsar, one can only estimate the strain field here at earth. Several mechanisms give upper bounds to the strength of GWs on earth. One such limit is the 'spin down limit', which is given by the observed spin-down rate of the pulsar, and the assumption that all of the rotational kinetic energy which is lost is in the form of GWs [16]. Another limit is given by the yield strength of the material which makes up the NS, and how much strain the crust can sustain before breaking apart due to centripetal forces [17, 18]. The presence of strong magnetic fields indicate a potential mechanism for producing and sustaining such strains due to deformation of the NS [19, 20]. However, without knowing the strength and direction of the internal magnetic fields in a pulsar, it is difficult to estimate a lower limit on the size of GW signal. The measurement of GWs from pulsars would therefore give us crucial information about the stellar interior.

Since pulsars should emit continuous and coherent GWs at specific and known frequencies, we can use a narrowband detector and integrate the signal for long times, averaging away the incoherent detector noise. We show that for reasonable parameters, the superfluid helium detector can approach strain sensitivities of $1 - 5 \times 10^{-23}/\sqrt{\text{Hz}}$ at around 1 kHz, depending on the size and Q factor of the detector. Pulsar frequencies are observed to vary slightly due to random glitches $\Delta f/f \sim 10^{-6} - 10^{-11}$ (older, MSPs being more stable) [21], and due to the motion of the Earth around the Sun and resulting doppler frequency shifts. The tunability of the acoustic resonance will be essential to track these shifts during long detection integration times. Simultaneous monitoring of the targeted pulsar electromagnetically can facilitate the required precision frequency tracking. The frequency agility can also allow for using the same acoustic resonator to look for signals from multiple pulsars.

Recent measurements with LIGO and Virgo have unsuccessfully searched for GW signals from 179 pulsars and have limited the strain field $h \lesssim 10^{-25}$ for most pulsars after nearly a year of integration time [22]. In a parallel development, hundreds of new pulsars have been discovered in the last few years by analyzing gamma-ray sources observed by the Fermi Large Area Telescope (Fermi-LAT), some less than 0.5 kpc from earth [23, 24]. Together, these developments accentuate the need for new technology for GW astronomy of pulsars.

This paper is organized as follows. We start with an overview of continuous GWs from pulsars to get an estimate for the strains produced on earth in section 2. We then describe the superfluid helium detector and show how it functions as a detector for GWs in section 3. In section 4, we provide the detection system requirements. We then compare this detector with other functional GW detectors, and show the key fundamental differences between these detectors and our proposed detector in section 5. Finally, we conclude with a summary of the key features of this detector and outlook in section 6. A review of the relevant concepts and derivations are relegated to the appendices for the interested reader.

2. Sources of continuous GWs

The generation of GWs can be studied by considering the linearized Einstein equations in the presence of matter [25]. The computations are similar to the analogous case in electromagnetism [26], see appendix A for a summary. However, in the absence of gravitational dipoles, a quadrupole moment Q_{ij} is necessary to source GWs. The emitted power of GWs is found to be [27]

$$P = \frac{G}{5c^5}\langle \ddot{Q}_{ij}\ddot{Q}^{ij}\rangle, \tag{1}$$

i.e. it depends on the third time derivative of the quadrupole moment of the system, where $Q_{ij} \coloneqq \rho \int_{\text{body}} x_i x_j \mathrm{d}V$ for a body of density ρ.

In the far-field limit where size of the source $(GM/c^2) \ll$ wavelength of the GW $(c/\omega) \ll$ distance to detector (d), the gravitational metric perturbation becomes

$$h_{ij} = \frac{2G}{c^4 d}\ddot{Q}_{ij}, \tag{2}$$

where h is the gravitational perturbation tensor in transverse-traceless gauge. Since $G/c^4 \sim 10^{-44}$ N s^4 kg^{-2}, one needs events with relativistic changes in quadrupole moment to have a measurable GW signal on earth. As an estimate, if all the observed slowdown of the Crab pulsar was converted into gravitational radiation, the power would correspond to $P \sim 4.5 \times 10^{31}$ W (10^5 times the electromagnetic radiation power from the Sun) [28]. However, at a distance 2 kpc away from the pulsar (distance to earth), the power flux is 10^{-9} W m^{-2} and the metric perturbation is $h \sim 10^{-24}$. Even though the power flux is macroscopic and easily detectable in other forms (acoustic, electromagnetic, etc), the resulting strain is very small due to the remarkably high impedance of space-time. This is at the heart of the difficulty with laboratory detection of GWs.

Estimates of gravitational radiation from pulsars is an active area of theoretical research that goes back to early observations of pulsars [15]. The mechanism for GW generation is assumed to be an asymmetric mass distribution. Several mechanisms are proposed for the deviation from axial symmetry in mass distribution, for example magnetic deformations [18], star quakes or instabilities due to gravitational or viscous effects [21, 29]. However, due to the unknown equation of state, there is significant variability in estimates of mass asymmetry and thus GW strain from pulsars.

We now estimate the GW perturbation strain from measured spin-down rates and briefly discuss the validity of this limit. We then present relevant numbers for a few MSPs of interest for our detector. Details about these derivations and typical parameters for other pulsars of interest are presented in appendix B.

For an ellipsoidal pulsar rotating about the z-axis with frequency ω_p, the two polarizations of h are given by

$$h_+ = -\frac{4G}{c^4 d}\epsilon I_{zz}\omega_p^2 \cos 2\omega_p t, \tag{3}$$

$$h_\times = \frac{4G}{c^4 d}\epsilon I_{zz}\omega_p^2 \sin 2\omega_p t, \tag{4}$$

where I_{zz} is the moment of inertia along the z-axis and ϵ characterizes the mass quadrupole ellipticity $(\epsilon = (Q_{xx} - Q_{yy})/I_{zz})$. The energy flux for a continuous GW of polarization A from a pulsar source is given by

$$s^A = \frac{c^3}{16\pi G}\overline{\dot{h}_A(t)^2}, \tag{5}$$

where $A \in \{+, \times\}$ and the bar indicates time-averaging.

Typical NSs have mass 1–1.5 $M_\odot$ (where $M_\odot = 2 \times 10^{30}$ kg is the solar mass) and have a radius of around 10 km. Using these values, the moment of inertia amounts to 10^{38} kg m^2, the estimate used in previous GW searches, see [22]. The ellipticity parameter is estimated by assuming that the observed slow-down rate $(\dot{\omega}_p)$ of a pulsar is entirely due to emission of GWs. This estimate is then used to compute the upper-limit estimate for gravitation perturbation strain known as the spin down strain,

$$h_{\text{sd}} = -\frac{4G}{c^4 d}\epsilon I_{zz}\omega_p^2 = \sqrt{\frac{5GI_{zz}\dot{\omega}_p}{2c^3 d^2 \omega_p}}. \tag{6}$$

Thus if we know the distance (d), rotational frequency (ω_p) and spin-down frequency $(\dot{\omega}_p)$ from astronomical observations, we can put limits on GW strain from pulsars.

While h_{sd} is a useful first-principles upper limit, it over-estimates the strength of GWs. This has already been confirmed by braking index measurements [30, 31] and the negative results from recent GW detector data [22]. However, long-lived and stable MSPs ($\omega_p/2\pi < 10^{-14}$ Hz s^{-1}) such as the ones considered here have been proposed as likely sources of continuous GWs [32]. The frequency stability and relatively low magnetic field

Table 1. Table of millisecond Pulsars with frequency greater than 500 Hz: ω_p is the rotational frequency, $f_{\rm GW} = \omega_p/\pi$ is the frequency of gravitational waves, $\dot{\omega}_p$ is the measured spin down rate, and d is the distance to the pulsar in kilo-parsecs, $h_{\rm sd}$ and $h_{\rm en}$ are the spin-down and elastic strain limits. These values are compared to the strain limit set by recent continuous GW surveys by LIGO+VIRGO $h_0^{95\%}$ [22, 34], and the strain limit for three identical Gen1 helium detectors operating at [020] mode with an integration time of 250 d (except for J1748 −2446ad, where mode [201] was used). Pulsars indicated by superscript * were discovered by the Fermi gamma ray telescope.

Pulsar	$\omega_p/2\pi$ (Hz)	$f_{\rm GW}$ (Hz)	$\dot{\omega}_p/2\pi$ (Hz s^{-1})	d (kpc)	$h_{\rm sd}$ $\times 10^{-25}$	$h_{\epsilon n}$ $\times 10^{-25}$	$h_0^{95\%}$ $\times 10^{-25}$	$h_{\rm He,1}^{95\%}$ $\times 10^{-25}$
J0034−0534	532.71	1065.43	-1.4×10^{-15}	1	1.3×10^{-2}	48	0.49	1.1×10^{-1}
J1301+0833*	542.38	1084.76	-3.2×10^{-15}	0.7	2.8×10^{-2}	71	1.1	1.1×10^{-1}
J1747−4036*	609.76	1219.51	-4.9×10^{-15}	3.4	6.7×10^{-3}	19	No data	9.2×10^{-2}
J1748−2446O	596.44	1192.87	-9.3×10^{-15}	5.9	5.4×10^{-3}	10	2.6	9.6×10^{-2}
J1748−2446P	578.50	1157	-8.9×10^{-14}	5.9	1.7×10^{-2}	9.6	1.6	1.0×10^{-1}
J1748−2446ad	716.36	1432.7	-1.7×10^{-14}	5.9	6.7×10^{-3}	15	1.8	3.3×10^{-1}
J1810+1744*	601.41	1202.82	-1.6×10^{-15}	2.5	5.3×10^{-3}	24	0.49	9.4×10^{-2}
J1843−1113	541.81	1083.62	-2.9×10^{-15}	2.0	9.4×10^{-3}	25	0.46	1.1×10^{-1}
J1902−5105*	574.71	1149.43	-3.0×10^{-15}	1.2	1.5×10^{-2}	47	No data	1.0×10^{-1}
J1939+2134	641.93	1283.86	-4.3×10^{-14}	1.5	4.4×10^{-2}	46	0.48	8.6×10^{-2}
J1959+2048	622.12	1244.24	-6.2×10^{-15}	1.5	1.7×10^{-2}	44	0.74	9.0×10^{-2}

indicate that unlike young pulsars like Crab and Vega, the dominant spin down mechanism in MSPs is more likely to be gravitational radiation.

We can also set limits on GW generation mechanism by considering specific models of the interior of NSs, as discussed in [29], and reviewed briefly in appendix B. Assuming standard nuclear matter and breaking strain for elastic forces, the ellipticity sustained can be limited to less than 4×10^{-6}, irrespective of the physics leading to deformations [18, 33]. This can also be used to evaluate the GW strain amplitude limit $h_{\epsilon n}$. Since the strain limits $h_{\rm sd}$ and $h_{\epsilon n}$ come from different physics (conservation of angular momentum and balancing forces in stellar interior), we use the lower of the two as the upper limit for metric strain.

Table 1 details parameters for pulsars of interest with rotational frequency higher than 500 Hz, along with current limitations on GW strain from the LIGO+VIRGO collaboration. Theoretical estimates of metric strain assuming spin-down limit, and elastic crust breakdown limit on ellipticity ($\epsilon = 4 \times 10^{-6}$) from [18] are also given. Table 1 also gives the strain estimate set by the helium detector outlined in figure 1 (Gen1) that we will discuss in detail in the following sections. Several of these pulsars were discovered recently by analyzing gamma-ray sources from Fermi-LAT. The number of known fast spinning pulsars is expected to grow significantly as more sources are discovered and analyzed.

Since the strain due to GWs from pulsars is expected to be very small but coherent, one needs to integrate the signal for a long time (the latest result being a compilation of ∼250 d of integration over three detectors [22]). Also, in order to rule out noise we need to detect a GW signal from at least two different detectors. Strain sensitivity also improves as $\sqrt{N_d}$, where N_d is the number of detectors [35]. There has been computationally intensive analysis of LIGO+VIRGO data to search for such GW signals. While being unsuccessful, they have improved the upper bound on the emitted wave amplitudes. In the following, we outline the proposal for a simple, low-cost, narrowband detector for these GW strains based on a superfluid helium optomechanical system. Being relatively simple and economical, superfluid helium detectors can be set up in multiple locations to improve overall detection sensitivity.

As a precursor to subsequent discussions, we present the central result of our work in figure 2, showing the limits set by different detectors for ten MSPs of interest from table 1. Along with the spin-down limit and limit set by the previous measurement [22], we also show the limits set by two different geometries of helium detectors that we discuss in detail in sections 3 and 4. Here, we have assumed that the resonance frequency of the same acoustic mode can be tuned by up to 200 Hz without changing the Q-factor (of 6×10^{10}), thereby resonantly targeting each pulsar with the same detector.

3. Superfluid helium GW detector

The GW strain detector we propose is a resonant mass detector formed by acoustic modes of superfluid helium in a cavity parametrically coupled to a microwaves in a superconducting resonator. For the purpose of our calculations, we will treat the superfluid as an elastic medium with zero dissipation. At the temperatures we expect to operate this detector, $T < 10$ mK, the normal fluid fraction ρ_n is expected to be $\rho_n/\rho_0 < 10^{-8}$, where ρ_0 is the total density of the fluid [37]. For temperatures below $T < 100$ mK, the dissipation of audio frequency acoustic waves is expected and found to be dominated by a three-phonon process, falling off as T^{-4}.

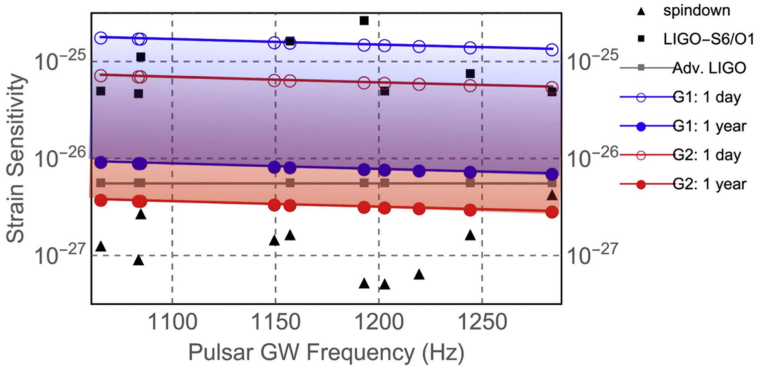

Figure 2. Strain sensitivity of various detectors for 10 MSPs of interest for the helium detector versus measurement time for two helium detectors with same sensitivity operating simultaneously, at a bath temperature of 5 mK, $[lmn] = [020]$, and Q-factor of 6×10^{10} for both Gen1 (mass = 2.66 kg, in blue) and Gen2 (mass = 15.9 kg, in red) detectors. We also show the current limits on strain set by LIGO+VIRGO collaboration [22, 34] and calculated limit of Advanced LIGO operating at design sensitivity for 365 d [36]. As seen in the figure, the current limit on pulsar GW strains can be surpassed within a few days of integration time for Gen1, and in under a few days for Gen2. Also shown is the spin-down limit for these pulsars.

An elastic body (with dimensions $\ll \lambda_{\rm GW}$) in a gravitational field will undergo deformation due to changes in space-time as a GW passes by. The equation of motion for the displacement field $\mathbf{u}(r,\ t)$ of an elastic body is given by [38]

$$\rho\frac{\partial^2\mathbf{u}}{\partial t^2} - \mu_{\rm L}\nabla^2\mathbf{u} - (\lambda_{\rm L} + \mu_{\rm L})\nabla(\nabla\ .\ \mathbf{u}) = \frac{1}{2}\rho\ \ddot{\mathbf{h}}\mathbf{x}, \tag{7}$$

where ρ is the density, $\lambda_{\rm L}$, $\mu_{\rm L}$ are the Lamé coefficients for the elastic body and $\ddot{\mathbf{h}}\mathbf{x}$ is the effective amplitude of the wave for a particular orientation of the detector that exerts an effective tidal force on the detector.

This acoustic deformation can be broken into its eigenmodes $\mathbf{u}(\mathbf{r},\ t) = \sum_n \xi_n(t)\mathbf{w}_n(\mathbf{r})$. For this analysis, we assume our acoustic antenna is in a single eigenmode of frequency ω_m, thus dropping index n. We have used the notation where $\mathbf{w}(\mathbf{r})$ is a dimensionless spatial mode function with unit amplitude, and the actual amplitude of the displacement field is in $\xi(t)$.

Rigid boundary walls and zero viscosity enables us to describe the acoustic modes accurately via a wave equation as opposed to Navier–Stokes equations typically used for fluid flow. The spatial modes are obtained by solving the acoustic equations of motion [39], as outlined in appendix C. These acoustic modes of helium in a superconducting cavity were experimentally studied by some of the authors in [4]. We found them to be well-modeled by this theory, and have Q-factors exceeding 10^8 at 45 mK.

For the purposes of this paper, we will simply add the finite linear dissipation to the acoustic resonance, parameterized as a finite Q. For a damped acoustic resonator, equation (7) can be simplified to show that the displacement field $\xi(t)$ satisfies the equation of motion [40, 41]

$$\mu\left(\ddot{\xi} + \frac{\omega_m}{Q_{\rm He}}\dot{\xi} + \omega_m^2\xi\right) = \frac{1}{4}\sum_{ij}\ddot{h}_{ij}q_{ij}, \tag{8}$$

where $Q_{\rm He}$ is the Q-factor and μ is the reduced mass for the particular eigenmode, $\mu = \int\rho\mathbf{w}^2{\rm d}V$, and q_{ij} is the dynamic part of the quadrupole moment,

$$q_{ij} = \int\rho\left(w_ix_j + x_iw_j - \frac{2}{3}\delta_{ij}\mathbf{w}\cdot\mathbf{r}\right){\rm d}V. \tag{9}$$

In their analysis of various antenna geometries for GW detection, Hirakawa and co workers introduced two quantities to compare GW antennas spanning different size and symmetry groups [41]. These are the effective area (A_G) characterizing the GW-active part of the vibrational mode, and the directivity function (d^A), which characterizes the directional and polarization dependence of the antenna. They are defined as

$$A_G = \frac{2}{\mu M}\sum q_{ij}^2 \tag{10}$$

and

$$d^A(\theta,\ \phi) = \frac{5}{4}\frac{\left(\sum q_{ij}e_{ij}^A(\mathbf{k})\right)^2}{\sum q_{ij}^2}, \tag{11}$$

where M is the total mass of the antenna and e_{ij}^A is the unit vector for incoming GW signal polarization A ($A \in \{+,\ \times\}$) in arbitrary direction $\mathbf{k}(\theta,\ \phi,\ \psi)$. The Euler angles $(\theta,\ \phi,\ \psi)$ transform from the pulsar

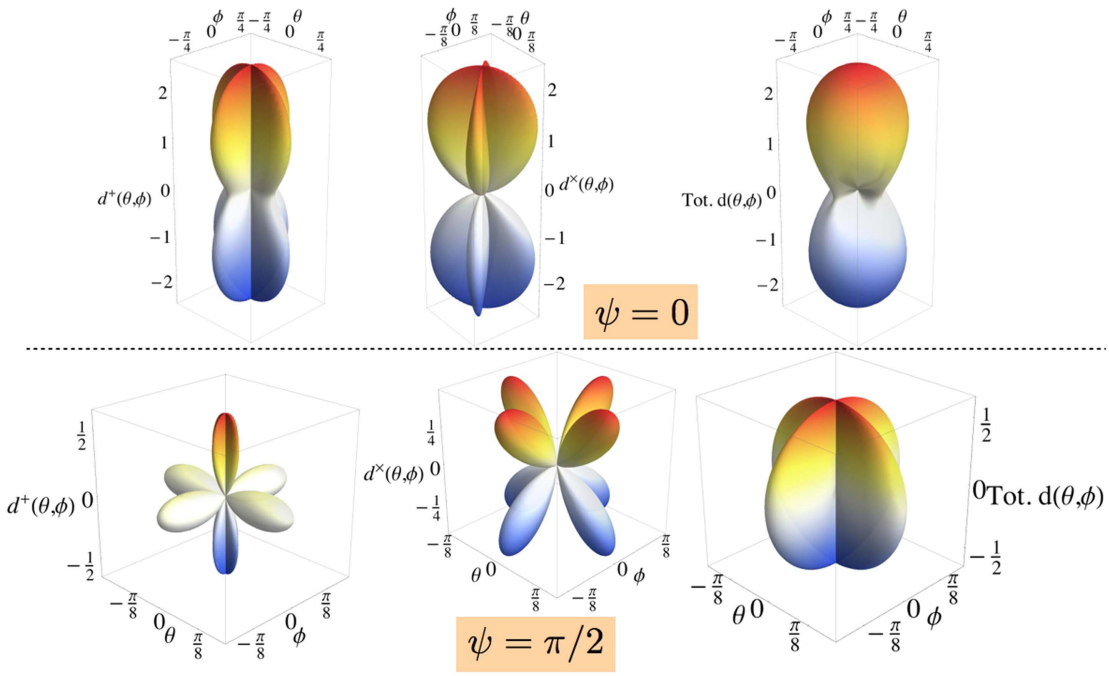

Figure 3. The directivity patterns for acoustic mode $[lmn] = [020]$ of the cylindrical cavity. The $+$, $\times$ polarization and total directivity functions are given for two different polarizations of the detector (Euler angle $\psi = 0,\ \pi/2$). The orientation of the detector can be adjusted to optimize the directivity function for the astrophysical source in consideration.

coordinate system to the detector co-ordinate system and are discussed in appendix A, along with the explicit form of e_{ij}^A. An important distinction between the proposed detector and other GW sensors, particularly the interferometric ones, is that the orientation of the detector (parameterized by ψ) can be adjusted to optimize the directivity function for the astrophysical source in consideration due to its small size. This acts as another tunable parameter that can give significant enhancement in sensitivity, as shown in figure 3 for mode [020].

In terms of the above expressions, the mean squared force from a continuous GW source of polarization A is

$$\overline{f_G^2} = \frac{2\pi G}{5c^3} M\mu\omega_G^2 A_G d^A(\theta,\ \phi)s^A = \frac{1}{40} M\mu\omega_G^4 A_G d^A \overline{h_A(t)^2}, \tag{12}$$

where $\omega_G = 2\omega_p$ is the GW frequency. Here we have assumed a δ-function GW spectrum.

As an example, we choose a cylindrical cavity of radius $a = 10.8$ cm, length $L = 50$ cm (from now onwards referred to as Gen1 or with subscript (He, 1)). We focus on the acoustic mode $f_{(0,2,0)} = 1071$ Hz, which has an effective mass $\mu = 0.625M$, and a large GR-active area of $A_G = 0.629\pi a^2$ due to its quadrupolar shape, shown in figure C1. Another geometry considered in this work is a cylindrical cavity of the same radius, but length $L = 3$ m (from now onwards referred to as Gen2 or with subscript (He, 2)). Since the resonance frequency of the [020] mode is independent of length, it remains unchanged. However, increasing the mass gives us a larger effective mass for the same area. Figure 3 shows the various directivity functions for this acoustic mode that capture the angular dependence of the sensitivity of the detector. Appendix C discusses several characteristics of the first few modes of the cylindrical cavity that have a non-zero quadrupolar tensor in more detail.

4. Noise mechanisms and minimum detectable strain

The system we are proposing and have been exploring in the laboratory [4, 6] is a parametric transducer [42] and essentially similar to other optomechanical systems [43]: the acoustic motion of the superfluid and resulting perturbation of the dielectric constant modulates the frequency of a high-Q superconducting microwave resonator. The details of the coupled acoustic and microwave system, sources of dissipation (phonon scattering, effect of isotopic impurities, radiation loss,) requirements on thermal stability, etc are the subject of another manuscript [6]. Here we take a few central results of this analysis.

The noise sources relevant to this system are the Brownian motion of the fluid driven by thermal/dissipative forces, the additive noise of the amplifier which is used to detect the microwave field, the added noise of the stimulating microwave field (phase noise), and possible back-action forces due to fluctuations of the field inside the microwave cavity (due to phase noise and quantum noise). The effect of vortices in superfluid helium due to

earth's rotation on the Q-factor is unclear. However, using an annular cylinder or an equatorial mount allows for long integration times without the possibly detrimental effects due to vortices.

Active and passive vibration isolation schemes deployed in interferometric sensors can be easily transplanted to our proposed detector. Seismic isolation requirements for this detector are less stringent than LIGO primarily due to the high frequency of operation (~1 kHz). Furthermore, due to the mismatch between the speed of sound in helium and niobium, there is natural acoustic isolation from the container. We will assume for the purpose of this discussion that the challenging job of seismically isolating the superfluid cell from external vibrations has been accomplished, as has been done for other GW detectors, including LIGO [44], cryogenic test masses for KAGRA [45], and various resonant detectors [46]. Due to the high frequency and narrow bandwidth of the astrophysical source of interest, the strain noise due to Newtonian gravity fluctuations are expected not to be relevant for this detector [44].

For a sufficiently intense microwave pump, with sufficiently low phase noise, the thermal Brownian motion of the helium will dominate the noise. Assuming the device is pumped on the red sideband, $\omega_{pp} = \omega_c - \omega_m$, and that the system is the side-band resolved limit, $\omega_m > \kappa_c$, the upconversion rate of microwave photons is given by: $\Gamma_{\rm opt} = 4(\Delta p_{\rm SQL} \cdot g_0)^2 n_p/\kappa_c$, where ω_{pp}, ω_c, and ω_m are the pump, cavity, and acoustic mode frequency respectively, $\kappa_c = \omega_c/Q_{\rm Nb}$ is the cavity damping rate, $\Delta p_{\rm SQL}$ is the amplitude of the zero-point fluctuation of the pressure of the acoustic field, n_p is the amplitude of the pump inside the cavity measured in quanta, and g_0 is the coupling between the acoustic and microwave field. For the geometry we consider here, Gen1: $l = 0.5$ m, $a = 0.108$ m, $\omega_m = 2\pi \times 1071$ Hz, $\omega_c = 2\pi \times 1.6$ GHz, and $g_0 = -2\pi \times 7.5 \times 10^{-11}$ Hz.

To achieve a readout with noise temperature of 1 mK, which means that the added noise of the amplifier is equal to the thermal noise amplitude when the helium is thermalized at 1 mK, requires $n_p = 6 \times 10^9$ microwave pump photons and a phase noise of -145 dB_c/Hz. To begin to dampen and cool the acoustic resonance with cavity backaction force, would require $n_p = 10^{12}$, and a phase noise of -145 dB_c/Hz. Microwave sources have been realized using sapphire resonators with phase noise of -160 dB_c/Hz at 1 kHz [47, 48]. To incorporate a similar low noise oscillator in our detector, one has to implement a microwave readout using interferometric frequency discriminator, as used in [49].Together with a tunable superconducting cavity, it is possible to realize a source with sufficient low noise to broaden and cool this mode with backaction, as demonstrated earlier in resonant bar antennas [50].

Due to the very low dielectric constant of helium ($\epsilon_{\rm He} = 1.05$), the bare optomechanical coupling constant is small compared to typical micro-scale optomechanical systems:
$g_0 = \Delta p_{\rm SQL} \cdot \partial\omega_c/\partial\Delta p = -2\pi \times 7.5 \times 10^{-11}$ Hz: this is the frequency shift of the Nb cavity, ω_c, due to the zero-point fluctuations of the acoustic field of the helium, $\Delta p_{\rm SQL}$. However, the relevant quantity is cooperativity, $C = \Gamma_{\rm opt}/\gamma_{\rm He}$, which compares the rate of signal photon up-conversion, $\Gamma_{\rm opt}$, to the loss rate of acoustic quanta to the thermal bath, $\gamma_{\rm He} = \omega_{\rm He}/Q_{\rm He}$. With quantum limited microwave detection (now possible with a number of amplifiers), detection at the SQL is achieved when $C = 1$, and is the onset of significant backaction effects such as optomechanical damping and cooling. The key point is that for this system we expect to be able to realize very large n_p. This is due to the very high Q possible in Nb, ($Q_{\rm Nb} \sim 10^{11}$ is now routine for accelerator cavities [51, 52], even when driven to very high internal fields of 10^7 V m^{-1} corresponding to $n_p = 10^{23}$,) and dielectric losses and resulting heating at microwave frequency in liquid helium are expected to be negligible up to very high pump powers. Assuming the dielectric loss angle in helium is less than 10^{-10}, our estimates suggest that $n_p = 10^{16}$ should be achievable before dissipative effects lead to significant heating of helium at 5 mK, far beyond the internal pump intensity used with micro-optomechanical systems and far above the onset of backaction effects, $C = 1$ for $n_p = 8 \times 10^{11}$. As a result, we are optimistic that SQL limited detection and significant backaction cooling and linewidth broadening are possible. As seen in other resonant GW antennas [50, 53], one has to be careful about amplitude noise of the pump, since it starts deteriorating the acoustic Q-factor at large powers due to backaction forces.

Since the frequency and phase of the pulsar's GW signal should be known through observations of the electromagnetic signal, single quadrature back-action evading, quantum non-demolition measurement techniques could be implemented [54]. This has the advantage of avoiding the back-action forces from the cavity field fluctuations and can lower the phase noise requirements of the microwave pump. Similar noise evasion techniques have already been studied in resonant GW antennas [55].

In the following discussion we assume that noise at the detection frequency is dominated by the thermal noise of the acoustic mode. As highlighted in the previous paragraphs, this assumption is valid for a sufficiently intense microwave pump, with sufficiently low phase noise. This involves implementing state of the art microwave transducer technology in our system. Detailed quantitative analysis of the contribution of various types of transducer noise to strain sensitivity will be the subject of future work. We also assume acoustic Q-factors of around 10^{10} in these calculations. While other low loss materials such as sapphire, quartz and silicon have demonstrated acoustic Q-factors higher than the one we demonstrated for superfluid helium (1.4×10^8), it appears possible for helium to reach significantly higher Q-factors than those measured so far with technical

Table 2. Table of millisecond Pulsars of interest for helium detectors Gen1 and Gen2. Here, ω_p is the pulsar rotational frequency, $f_{\rm GW} = \omega_p/\pi$ is the frequency of GWs, as given in table 1. These values are compared to the strain limit set by recent continuous GW survey by interferometric detectors [22, 34], along with the strain limit for the helium resonant detectors Gen1 with an integration time of 250 d and Gen 2 with one year integration time, as shown in equation (15). Here, $\psi = 0$, Q-factor is 6×10^{10}, and the acoustic mode is given in square brackets.

Pulsar	$\omega_p/2\pi$	$f_{\rm GW}$ (Hz)	$h_{\rm sd}$	$h_0^{95\%}$- LIGO	$h_{\rm He,1}^{95\%}(l,m,n)$	$h_{\rm He,2}^{95\%}(l,m,n)$
J0034−0534	532.71	1065.43	1.3×10^{-27}	4.9×10^{-26}	1.1×10^{-26}[020]	3.8×10^{-27}[020]
J1301+0833	542.38	1084.76	2.8×10^{-27}	1.1×10^{-25}	1.1×10^{-26}[020]	3.7×10^{-27}[020]
J1843−1113	541.81	1083.62	9.4×10^{-28}	4.6×10^{-26}	1.1×10^{-26}[020]	3.7×10^{-27} [020]
J1748−2446ad	716.36	1432.7	6.7×10^{-28}	1.8×10^{-25}	3.3×10^{-26}[201]	No coupling

improvements like lowering the temperature and using an isotropically purified helium sample, as we detail in [6]. This is due to the fact that in the low loss solids mentioned above, the acoustic Q-factor seems to be limited by point defects and dislocations in the crystal lattice [56]. Our proposed resonant antenna is not expected to suffer from these loss mechanisms due to unique properties of superfluid ^{4}He. This makes us optimistic about attaining the extremely high Q factors used in this theoretical work in the long run.

At effective temperature T, the force noise spectral density S_{FF} is given by the relation $S_{\xi\xi}[\omega] = |\chi(\omega)|^2 S_{FF}[\omega]$, with the susceptibility $\chi(\omega) = [\mu((\omega_m^2 - \omega^2) + i\gamma_{\rm He}\omega)]^{-1}$, and the position noise spectral density is given by

$$S_{\xi\xi}^{\rm th}[\omega] = \frac{k_B T}{\mu\omega_m^2}\left\{\frac{\gamma_{\rm He}/2}{(\omega+\omega_m)^2 + \gamma_{\rm He}^2/4} + \frac{\gamma_{\rm He}/2}{(\omega-\omega_m)^2 + \gamma_{\rm He}^2/4}\right\}, \tag{13}$$

with $\gamma_{\rm He} = \omega_m/Q_{\rm He}$. For gravitational strain, using equation (8), we find $S_{hh}[\omega] = 40 S_{FF}[\omega]/(\mu M \omega_G^4 d^A A_G)$ for a continuous GW source at frequency ω_G. Combining these, we find that for a resonant mass detector at $\omega_G = \omega_m$,

$$S_{hh}[\omega] = \frac{80 k_B T}{M d^A A_G Q_{\rm He} \omega_m^3}. \tag{14}$$

The strain sensitivity of our detector is simply $\sqrt{S_{hh}[\omega]}$, and the minimum noise is $\sqrt{S_{hh}[\omega]/\tau_{\rm int}}$ after an integration time $\tau_{\rm int}$. The minimum detectable strain field with 2σ certainty is therefore given by [32]

$$h_{\rm min} \approx 2\sqrt{\frac{S_{hh}[\omega]}{\tau_{\rm int}}} = \sqrt{\frac{320 k_B T}{M\omega_G^3 A_G d^A Q_m}\frac{1}{\tau_{\rm int}}}. \tag{15}$$

The 2σ limit is used to be consistent with previously reported limits on $h_{\rm min}$ [22].

As an example, both cylindrical cavities considered in section 3 have acoustic mode $f_{[0,2,0]} \sim 1071$ Hz. This mode of the detector can easily be tuned (by under ± 15 Hz) to be in resonance with pulsars J0034−0534, J1301+0833, and J1843−1113. Similarly, another acoustic mode ($f_{[2,0,1]} = 1425$ Hz) is found to have resonant frequencies in the vicinity (<8 Hz) of the frequency of GWs from pulsar J1748−2446ad. Taking into account the different quadrupole tensors, effective mass and directivity functions for the different acoustic modes (discussed in appendix C), table 2 lists the minimum detectable strain for these pulsars for cylindrical detector Gen1 after 250 d of integration time (same time as in [22]). Here we have assumed an acoustic Q-factor of 6×10^{10} and thermal $T = 5$ mK for both geometries. Since the detector is small enough to be rotated or moved geographically to optimize signal from a particular pulsar, we have assumed $\psi = 0$ and (θ, ϕ) that maximizes the directivity.

In order to compare the sensitivity of our proposed detector with other GW sensors, we pick a specific expected astrophysical source: GWs from pulsar J1301+0833, with $\omega_G = 2\pi \times 1084.76$ Hz. Gen1 (mode [020]) gives us sensitivity of $h_{\rm min} = 4.4 \times 10^{-23}/\sqrt{\rm Hz}$, which is significantly below the sensitivity of LIGO, and comparable (within a factor of 3) to current sensitivity of advanced LIGO. Such a detector can surpass the LIGO+VIRGO estimate on minimum strain $h_0^{95\%} = 1.1 \times 10^{-25}$ in under a week of integration time (under a month if Q-factor is 6×10^9 instead). Increasing the mass by a factor of 6 (by choosing Gen2), while assuming the same Q-factor and noise characteristics, we can get sensitivity of $1.8 \times 10^{-23}/\sqrt{\rm Hz}$, which is below the strain sensitivity of advanced LIGO for this frequency range. Figure 4 shows the minimum detectable strain as a function of integration time for various Q factors for two resonant detectors operating at the same sensitivity. Figure 4 also shows the sensitivity estimates for three interferometeric detectors operating at LIGO-S6 sensitivity, and at advanced LIGO design sensitivity, as used in [22].

As figure 4 and table 2 demonstrate, Gen2 can come within a factor of 2 of the spin-down limit for pulsar J1301+0833 (and several other pulsars) in a year of integration time. Considering the conjecture that the primary spin-down mechanism for MSPs is the emission of gravitational radiation, our detector seems a promising candidate for searches of continuous GWs from this and similar other pulsars.

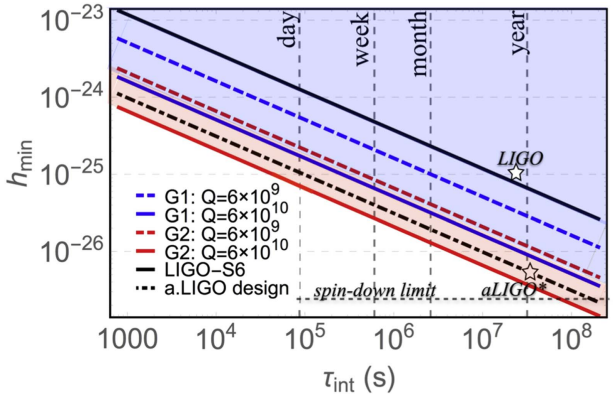

Figure 4. Strain sensitivity versus measurement time for two helium detectors with same sensitivity operating simultaneously, assuming a bath temperature of 5 mK, $(l, m, n) = (0, 2, 0)$, for Geometry 1(blue) and 2(red). We also show the limits set by three interferometric detectors operating at LIGO-S6 sensitivity (solid black), and the design sensitivity of advanced LIGO (dashed black). The stars shows the current limit on minimum strain set by LIGO, and the projected limit by Advanced LIGO. As seen in the figure, the current limit can be surpassed within a few days of integration time for Gen1, and under a day for Gen2. Also shown is the spin-down limit for pulsar J1301+0833.

We would like to note that several noise suppression mechanisms (such as squeezed light injection) currently used in LIGO can also be employed here. More importantly, there are ways to squeeze the mechanical motion of the detector [57–59]. This can significantly relax the size, Q-factor and microwave noise requirements, increasing the sensitivity of our proposed detector significantly. For example, exploring methods to squeeze mechanical motion by changing the speed of sound periodically, and exploring other effects arising from parametric coupling between the helium acoustic modes and the microwave resonator container is a straight forward extension of the current setup, since the helium is already being pressurized and parametrically coupled to microwaves for resonant force detection. A detailed analysis of implementing these protocols for improved GW sensing will be the subject of future research.

5. Comparison with other detectors

The basic principle of the superfluid helium detector is analogous to that of other resonant mass sensors, such as Weber bars. The use of resonant mass GW detectors has a 50 year history, dating back to early experiments by Weber [5]. There have been several proposals of using resonant mass detectors to search for GW from pulsars [32], and a few continuous GW searches targeting specific pulsars [60]. Here we highlight several key differences in the implementation using superfluid helium.

- Mass: We discuss a kg-scale sample of helium which is 10^3 times smaller than the typical resonant bar detectors. The low mass limits the utility of the helium detector to CW sources, whereas the massive detectors are useful for broadband impulse sources (such as the ones detected by LIGO). Nonetheless, there is high sensitivity for CW sources and the low mass makes a helium detector economical and small scale. One could deploy a few such detectors to seek coincidence and further improve sensitivity.
- $T/Q_{\rm He}$ temperature and quality factor: It is possible to cool an isolated sample of helium to temperatures less than 10 mK and we are anticipating very low loss. For instance, helium at 25 mK with $Q_{\rm He} = 10^9$ has a ratio $T/Q_{\rm He}$ 10^3 times smaller than the best value found in the literature, and potentially 10^6 times smaller at lower temperature [6].
- Optomechanical damping: It appears possible to substantially increase the acoustic resonance linewidth without decreasing the force sensitivity by parametrically coupling to microwaves [4]. While parametric transducers are also used in other resonant mass detectors [61, 62], the particular geometry and mechanism used in helium detector is expected to have lower noise characteristics [6].
- Frequency tunability: It is possible to change the speed of sound in helium by 50% by pressurization. This allows the apparatus to be frequency agile; thus searching several pulsars with the same detector. It also allows for long term tracking the same pulsar in the presence of deleterious frequency shifts. For example, the estimated Doppler shift of the GW signal from Crab pulsar is ~30 mHz $\rm yr^{-1}$ due to earth's motion. Our

detector can be tuned to track this shift, allowing for months of integration time, reducing SNR, and thereby the detection threshold.

A standard figure of merit used in literature to compare various bar detectors of different materials is $\eta = Q\rho c_s^3$ as mentioned in [63]. Typical values of η range from 10^{21}–10^{24} kg s^{-3}. According to this metric, helium may seem like a poor choice for a bar detector, ($\eta \sim Q_{\rm He} \times 10^9$ kg s^{-3}). This figure of merit is made of the material specific parameters in the minimum detectable strain, as given in equation (15). However, adding the temperature dependence, and large Q-factors make the helium sensor comparable to the resonant bar detector. In addition, due to its smaller size, temperature stability, seismic and acoustic isolation are much easier to maintain.

Unlike interferometric detectors like LIGO conducting a broadband search for GWs, the helium detector is narrowband, and will work best for detection of continuous coherent waves such as those from pulsars. Nevertheless, as highlighted in figure 4, around 1 kHz the setup described above has strain sensitivity within a factor of 4 (for Gen 1), or in principle even surpassing the sensitivity of advanced LIGO by considering a larger volume of superfluid helium (as done in Gen 2). This allows us to surpass the limits from previous CW searches of VIRGO+LIGO experiments ($h_{\rm min} \sim 10^{-25}$) within a week, or less depending on the detector size and Q-factor.

There are several ongoing and proposed detectors for GWs, for example space-based interferometric detector eLISA [11, 64], atom interferometry based detector AGIS-LEO [65], and Pulsar Timing Arrays [66]. These detectors operate at different frequency ranges, typically much lower than the helium detector considered here. As is the case for astrophysical sources of electromagnetic waves, the power spectrum of GWs is extremely broad and would require the use of different types of 'GW telescopes'. The astrophysical sources of interest for the helium detector are different from these other proposed detectors.

Finally, an important advantage of considering superfluid helium as a resonant GW sensor is that by designing different geometries and exploring different types of resonances, one could build detectors for a range of astrophysical sources. For example, by considering smaller containers or Helmholtz resonances in micro or nano-fluidic channels [67], it may be possible to build a resonant detectors for high frequency sources of GWs as explored in other devices [68, 69]. Alternatively, larger containers or low-frequency Helmholtz resonances may be used to detect continuous GWs from young pulsars or binary systems. Since the technology required for the proposed superfluid helium GW detector is space-friendly, it may be possible to design detectors for space missions if seismic noise becomes a deterrent.

6. Conclusions and outlook

As discussed in section 4, there are several stringent requirements for low-noise operation of our proposed detector: isotopically pure sample, sub-10 mK cryogenic environment, very low phase-noise microwave source, and vibration isolation. Furthermore, due to the low density and speed of sound, a reasonable size (∼1 m) bar detector made of helium can only be used for detection of continuous GWs.

Despite these extreme requirements, using superfluid ^{4}He does have several advantages. The low intrinsic dissipation and dielectric loss and wide acoustic tunability are direct manifestations of the inherent quantum nature of the acoustic medium. Since the container itself is in a macroscopic quantum state (superconductor), it further contributes to the extremely low-noise and high sensitivity nature of the proposed device by making an extremely high Q microwave resonator with very high power-handling.

Several ideas for future work are outlined in the manuscript at various places. They include investigating more complex geometries for stronger coupling to gravitational strain, or investigating other high-Q acoustic resonances (Helmholtz resonances) to detect other sources of continuous GWs. Also, many ideas from quantum optics and quantum measurement theory can be implemented here to increase bandwidth or sensitivity. For example, by periodically modulating the resonance frequency, it will be possible to upconvert out of resonance signals into helium resonance signals, thereby increasing the frequency tunability. Several techniques from quantum measurements can be applied to our proposed transduction scheme to avoid measurement backaction or to squeeze acoustic noise, thereby increasing the sensitivity further.

Even without these techniques, the extreme displacement sensitivity ($\sim 10^{-23}/\sqrt{\rm Hz}$) of this meter-scale device corresponds to a measurement of the width of milky way to cm-scale precision! This is again made possible by combining two macroscopic quantum states in the measurement scheme (a superfluid coupled to a superconductor). The resulting hybrid quantum sensor is an extremely low noise detector due to the robustness of the quantum states involved. As these experiments develop, a more broadly functioning GW detector may become realistic, as well as the detection of other extremely small laboratory-scale forces.

Acknowledgments

We would like to acknowledge helpful conversations with Rana Adhikari, Yanbei Chen, Dan Lathrop, Keith Riles, John Ketterson, Pierre Meystre, Jack Harris, David Blair and Nergis Mavalvala. We acknowledge funding provided by the Institute for Quantum Information and Matter, an NSF Physics Frontiers Center (NSF IQIM-1125565) with support of the Gordon and Betty Moore Foundation (GBMF-1250) NSF DMR-1052647, DARPA-QUANTUM HR0011-10-1-0066, the NSF ITAMP grant, and Army Research Office.

Appendix A. Brief introduction to GWs

GWs are solutions to the linearized Einstein equations, where the perturbed metric can be written as $g_{\mu\nu} = \eta_{\mu\nu} + h_{\mu\nu}$. Here, $\eta_{\mu\nu} = \mathrm{diag}[-1, 1, 1, 1]$ is the Minkowski metric and $|h_{\mu\nu}| \ll 1$ is a small perturbation of the metric. In free space, Einstein's equations of motion, which describe the dynamics of space-time, reduce to $R_{\mu\nu} = 0$, where $R_{\mu\nu}$ is the Ricci-tensor constructed from the metric. Since only the weak-field limit is considered, terms that are of higher order in $h_{\mu\nu}$ can be neglected. In addition, general relativity has an inherent gauge freedom related to the choice of coordinates. In the Lorentz-gauge the equations of motion reduce to a wave equation as in electromagnetism:

$$R_{\mu\nu} = \Box h_{\mu\nu} = (-\partial_t^2 + c^2\nabla^2)h_{\mu\nu} = 0. \tag{A.1}$$

This is the wave equation for GWs, which are small perturbations of flat space-time that propagate at the speed of light. A general plane-wave solution has the form $h_{\mu\nu}(\vec{x}, t) = A_{\mu\nu}\cos(\omega t - \vec{k}\cdot\vec{x} + \varphi)$, with the dispersion relation $\omega = c|\vec{k}|$. Choosing the specific transverse-traceless gauge, and a coordinate system in which the wave propagates only in the z-direction, the only non-vanishing components of the GW tensor are the spatial components

$$h_{ij} = h_+\left(t - \frac{z}{c}\right)\mathbf{e}_{ij}^{+}(\hat{z}) + h_\times\left(t - \frac{z}{c}\right)\mathbf{e}_{ij}^{\times}(\hat{z}), \tag{A.2}$$

where h_+ and $h_\times$ are the two polarization components with the polarization tensors given by

$$\mathbf{e}^{+}(\hat{\mathbf{z}}) = \begin{pmatrix} 1 & 0 & 0 \\ 0 & -1 & 0 \\ 0 & 0 & 0 \end{pmatrix} \tag{A.3}$$

and

$$\mathbf{e}^{x}(\hat{\mathbf{z}}) = \begin{pmatrix} 0 & 1 & 0 \\ 1 & 0 & 0 \\ 0 & 0 & 0 \end{pmatrix}. \tag{A.4}$$

GWs carry energy and have observable effects on matter. For test particles at a distance much shorter than the wavelength of the GW, the wave induces an effective time-dependent tidal force. To see this, it is convenient to use gauge-invariant quantities, such as the Riemann tensor which is invariant to linear order. Its only non-vanishing component is $R_{\mu 0\nu 0} = -\frac{1}{2}\ddot{h}_{\mu\nu}$, where the dot denotes differentiation with respect to coordinate time t. The Riemann tensor captures how neighboring geodesics (i.e. world lines of free particles) change with respect to each other: the vector x^μ that connects two geodesics follows the geodesic deviation equation $\ddot{x}^\mu = R^\mu_{0\nu 0}x^\nu = -\frac{1}{2}\ddot{h}_{\mu\nu}x^\nu$. This equation holds for geodesics that are close to each other as compared to the wave length λ of the GW, i.e. $x \ll \lambda$. From this equation follows the equation of motion for the distance between two neighboring test particles:

$$\ddot{x} = \frac{1}{2}(\ddot{h}_+ x + \ddot{h}_\times y),\ \ddot{y} = \frac{1}{2}(\ddot{h}_\times x - \ddot{h}_+ y). \tag{A.5}$$

The equations of motion are equivalent to the presence of an effective tidal force $F_i = \ddot{h}_{ij}x^j/2$ that acts on the particles. The corresponding effective force is conservative and can therefore be represented by force lines, shown in figure A1 for a purely plus-polarized wave. For a general polarization, the force line diagram is rotated counter-clockwise by the angle Ψ where $\tan(2\Psi) = \ddot{h}_\times/\ddot{h}_+$.

For only a plus-polarized wave ($h_\times = 0$), the solution to lowest order in h is

$$x(t) = x(0)\left(1 + \frac{h_+(t)}{2}\right) y(t) = y(0)\left(1 - \frac{h_+(t)}{2}\right). \tag{A.6}$$

The distances between nearby points oscillate in the x- and y-directions, i.e. perpendicular to the GW. A cross-polarized wave has the same effect but with the x–y-plane rotated by $\pi/4$.

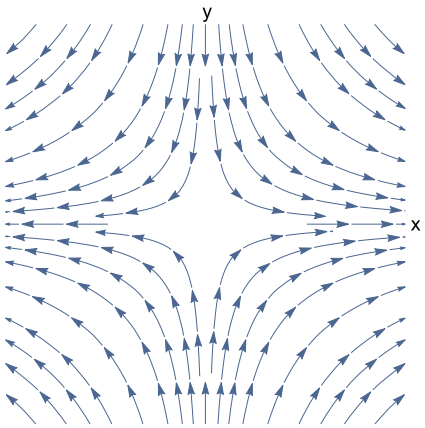

Figure A1. Force lines for the effective tidal force produced by a plus-polarized gravitational wave. The force acts perpendicular to the direction of propagation of the wave. The same force lines, rotated counter clock-wise by $\Psi = \pi/4$, represent the effect of a cross-polarized wave.

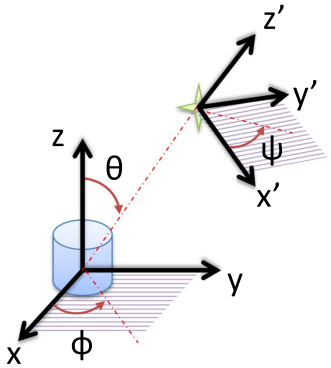

Figure A2. The co-ordinate transformation angles from the detector frame (symbolized by the cylinder) to the source frame (symbolized by the star). The angle Ψ in the x'–y'-plane defines the polarization of the gravitational wave.

The detector co-ordinate axis $(x,\ y,\ z)$ is not necessarily aligned with the gravitational wavefront emitted from the source $(x',\ y',\ z')$. To account for the angular dependence, the strain at the detector can be written as

$$h(t) = F_{+}(\theta,\ \phi,\ \psi)h_{+}(t) + F_{\times}(\theta,\ \phi,\ \psi)h_{\times}(t), \tag{A.7}$$

where $(\theta,\ \phi,\ \psi)$ are the Euler angles that convert from the pulsar co-ordinate system to the detector plane, as shown in figure A2, and $F_{+/\times}(\theta,\ \phi,\ \psi)$ are known as the detector pattern functions [70]. While the angles θ and ϕ describe the direction of the incoming GW (ϕ being rotation of the old x–y plane along the z-axis, and θ being the angle between the source and detector z-axis), ψ defines the polarization (rotation of the x–y plane along source line of sight) [71], as shown in figure A2. Compared to large ground-based sensors where the angle ψ is fixed, it can be used as a parameter for the helium detector, to be optimized for the particular pulsar in consideration.

Detector pattern function is defined as $F_A(\theta,\ \phi,\ \psi) = q_{ij}\hat{e}_A^{ij}(\theta,\ \phi,\ \psi)$, where $\mathbf{q}$ is the dynamic mass quadrupole tensor of the detector that we discuss below, and $\hat{e}_A^{ij}(\theta,\ \phi,\ \psi)$ (with $A \in \{+,\ \times\}$) are the unit vectors for the two polarizations of the GW given in equations (A.3), (A.4) in the rotated basis, $\hat{e}_A(\theta,\ \phi,\ \psi) = R_{XYZ}^{-1}\hat{e}_A R_{XYZ}$, where the rotation matrix is given by

$$R_{XYZ}(\theta,\ \phi,\ \psi) = \begin{bmatrix} \cos\theta\cos\phi & \cos\theta\sin\phi & -\sin\theta \\ -\cos\psi\sin\phi + \cos\phi\sin\theta\sin\psi & \cos\phi\cos\psi + \sin\phi\sin\theta\sin\psi & \cos\theta\sin\psi \\ \cos\phi\cos\psi\sin\theta + \sin\phi\sin\psi & \cos\psi\sin\theta\sin\phi - \cos\phi\sin\psi & \cos\theta\cos\psi \end{bmatrix}.$$

Appendix B. GW perturbation from an ellipsoidal pulsar

Let us assume a non-spherical pulsar, rotating about the z-axis with angular frequency ω_p. We assume an ellipsoidal star with the axes coinciding with the principal axes of the solid of revolution, with $a,\ b,\ c$ being the

semi-axes along x, y, z directions respectively. We also assume a constant mass density, ρ. The quadrupolar mass tensor is defined as $Q_{ij} \coloneqq \rho \int_{\text{body}} x_i x_j \mathrm{d}V$. Due to the (chosen) co-ordinate system being along the principal axes here, $Q = (1/5) M_p \,\text{diag}[a^2,\ b^2,\ c^2]$, where M_p is the mass of the pulsar. Assuming at time $t = 0$, $Q(t = 0) = \text{diag}[Q_1,\ Q_2,\ Q_3]$. Defining $Q = Q_1 + Q_2$, and ellipticity $\epsilon = (Q_1 - Q_2)/I_{zz}$, where $I_{zz} = (1/5) M (a^2 + b^2)$ is the moment of inertia about the z-axis [72], the quadrupolar tensor can be written as

$$Q = \begin{bmatrix} \frac{1}{2}Q + \frac{1}{2}\epsilon I_{zz} \cos 2\omega_p t & -\frac{1}{2}\epsilon I_{zz} \sin 2\omega_p t & 0 \\ -\frac{1}{2}\epsilon I_{zz} \sin 2\omega_p t & \frac{1}{2}Q - \frac{1}{2}\epsilon I_{zz} \cos 2\omega_p t & 0 \\ 0 & 0 & Q_3 \end{bmatrix}. \tag{B.1}$$

In the far-field limit, where size of the star (or GM/c^2) $\ll$wavelength of the GW (c/ω_p) $\ll$distance to detector (d), the GW perturbation becomes

$$h_{ij}(t,\ x) = \frac{2G}{c^4 d} \ddot{Q}(t_r), \tag{B.2}$$

where h is the gravitational perturbation tensor in transverse-traceless gauge, and $t_r = (t - d/c)$ is the retarded time, given the detector is distance d away from the source. Since time retardation gives an extra overall phase here, we ignore it for our purposes. Thus,

$$h = \frac{2G}{c^4 d} 2\epsilon I_{zz} \omega_p^2 \begin{bmatrix} -\cos 2\omega_p t & \sin 2\omega_p t & 0 \\ \sin 2\omega_p t & \cos 2\omega_p t & 0 \\ 0 & 0 & 0 \end{bmatrix}. \tag{B.3}$$

We now estimate the value of h for a typical pulsar in terms of astronomical observables. There are two unknowns here, I_{zz} and ϵ. These parameters depend on the composition of the NS. Even though the equation of state (relation between density and pressure) of a NS is unknown, certain properties of NSs are remarkably well understood, and agree with astronomical observations. Most models show that the radius lies between 10.5 and 11.2 km and mass ranges between $0.5 M_\odot$ and $3 M_\odot$, with all measured values close to $1.35 M_\odot$ (from Keplerian analysis of pulsars in binary systems- 5% of all observed pulsars) [21]. Putting in these values, the moment of inertia amounts to 10^{38} kg m^2, the estimate used in previous GW searches, see [22].

The biggest uncertainty in estimating h therefore stems from ϵ, the ellipticity parameter that characterizes the mass asymmetry of the pulsar. We now present estimates on ϵ from two different mechanisms: the spin-down energy conservation (ϵ_{sd}) and elastic strain on the NS crust (ϵ_n) and their corresponding GW strain limits.

Spin-down limit: Since the pulsar is spinning down, its rotational frequency is changing at some observable rate $\dot{\omega}_p$. This amounts to a torque of $I_{zz}\dot{\omega}_p$. We assume that all of this spin-down is due to gravitational radiation, $I_{zz}\dot{\omega}_p = \mathrm{d}L_z/\mathrm{d}t = (1/\omega_p)\mathrm{d}E/\mathrm{d}t$, where L_z is the angular momentum of the body along z axis, and E is the rotational kinetic energy. The emitted power of gravitational radiation is given by [27, 72]

$$\frac{\mathrm{d}E}{\mathrm{d}t} = \frac{G}{5c^5} \langle \dddot{Q}_{ij} \dddot{Q}^{ij} \rangle = \frac{32G}{5c^5} \epsilon^2 I_{zz}^2 \omega_p^6. \tag{B.4}$$

Solving for the ellipticity parameter, we find

$$\epsilon_{\text{sd}} = \left(\frac{5c^5 \dot{\omega}_p}{32 G I_{zz} \omega_p^5} \right)^{1/2}. \tag{B.5}$$

This in turn is used to compute the upper-limit estimate for gravitation perturbation strain in terms of constants and observational data

$$h_{\text{sd}} = -\frac{4G}{c^4 d} \epsilon I_{zz} \omega_p^2 = \sqrt{\frac{5 G I_{zz} \dot{\omega}_p}{2c^3 d^2 \omega_p}}. \tag{B.6}$$

The spin-down strain estimate is a significant over-estimate of the strength of GWs, particularly from young pulsars, as is eluded to by braking index measurements [30, 31], and also confirmed by the absence of GW signal in recent LIGO+VIRGO analysis [22].

This work primarily concerns a second class of pulsars, known as MSPs that are much longer-lived, slowly decaying, even speeding up at times. MSPs are remarkably stable ($\dot{\omega}_p/2\pi < 10^{-14}$ Hz s^{-1}) and were once considered strong candidates for long-term time-standards. There has only been one observed random glitch in the thousands of years of accumulated observation time [73]. This electromagnetic stability indicates that that gravitational radiation might dominate over magnetic dipole radiation as the dominant energy loss mechanism in MSPs.

Crustal strain limit: There are several mechanisms that contribute to the mass asymmetry. The NS's rotation and magnetic axis might not coincide, leading to an asymmetric mass distribution due to the enormous Lorentz forces. Alternatively, the mass distribution could also be changed significantly due to star quakes, internal magnetic fields, instabilities induced by gravitational effects, or viscosity of the dense matter [21]. Estimating the maximum elastic deformation sustained by a NS is an active field of research, see [29, 74], and references therein for details.

Ushomirsky *et al* set limits on the maximum quadrupole moment for a NS in the presence of elastic forces, irrespective of the nature of strain on the crust [33]. For standard parameters for I_{zz} and breaking strain of the crust, this quadrupole moment leads to a maximum ellipticity of $\epsilon_n \sim 4 \times 10^{-6}$ for a conventional NS [18]. This in turn can be used to evaluate the limit on the GW strain amplitude,

$$h_{\epsilon n} = -\frac{4G}{c^4 d}\epsilon_n I_{zz}\omega_p^2. \tag{B.7}$$

Both the spin down and strain mechanisms considered here put upper limits on the metric perturbation due to different physics. Therefore, we assume that the strain due to GW from pulsars is smaller than the lower of the two limits. For the younger pulsars with small rotation frequencies and large spin down rates, the upper limit on GW strain is set by the elastic deformation limit, while for MSPs smaller spin-down rates lead to a significantly lower limit set by $h_{\rm sd}$, as shown in table 1. In both cases, the GW signal limit is typically below 10^{-27}. While we have ignored magnetic deformations as the primary mass asymmetry mechanism in this work, for slower MSPs ($f_{\rm GW} < 0.1$ kHz) one of the most promising GW emission mechanisms is considered to be magnetic mountains formed by polar magnetic burial during accretion [20, 75].

These limits provide an upper limit on GW strength due to different physics, it is possible (in fact expected) that the actual signal would be even lower. However, it is worth stressing that the observation (or even absence) of a GW signal is the only known way to gain information about the interior of these exotic objects.

Appendix C. Search for optimal detector geometry

C.1. Acoustic modes of helium in cavity

For elastic deformations in enclosed spaces, the change of pressure $p(\mathbf{r})$ is described by

$$\nabla^2 p - \frac{1}{c_s^2}\frac{\partial^2 p}{\partial t^2} = 0 \tag{C.1}$$

with the speed of sound in the material (here helium) being c_s. The particle velocity $\mathbf{v} = \dot{\mathbf{u}}$ is related to pressure via $\partial\mathbf{v}/\partial\mathbf{t} = -\nabla\mathbf{p}/\rho$. Thus each vector component of the velocity $\mathbf{v}$ also satisfies the same wave equation as the pressure, but the components are not independent of each other. The full solution can be equivalently expressed in terms of the Helmholtz potential for the velocity, $\mathbf{v} = \nabla\Phi(\mathbf{r})$. In terms of the potential, the acoustic pressure becomes $p = -\rho\partial\Phi/\partial t$, and the potential satisfies the same wave equation

$$\nabla^2\Phi - \frac{1}{c_s^2}\frac{\partial^2\Phi}{\partial t^2} = 0. \tag{C.2}$$

As before, the time dependence can be explicitly separated via $\Phi \rightarrow \Phi(\mathbf{r})\xi(t)$. For cylindrical symmetry the solution for the spatial part of the potential is

$$\Phi(r,\,\theta,\,z) = J_m(k_m(n)r)\cos(m\theta)\cos\left(k_z(l)\left(z + \frac{L}{2}\right)\right), \tag{C.3}$$

where the wavevectors are found from the rigid boundary conditions $\partial\Phi/\partial z = 0$ at $z = \pm L/2$ and $\partial\Phi/\partial r = 0$ at r = a, such that $k_z(l) = l\pi/L$ with $l = 0,\,1,\,2\ldots$ and $k_m(n)$ follows from the n roots of $J'_m(k_m(n)a) = 0$. Having the solution for the potential, one can obtain the velocity vector field, and thus the spatial modes, via $\mathbf{w}(r,\,\theta,\,z) = \nabla\Phi(r,\,\theta,\,z)/|\mathbf{w}_{\rm max}|$, where $|\mathbf{w}_{\rm max}|$ is the maximum value of $\nabla\Phi(r,\,\theta,\,z)$. Figure C1 shows the first few modes of the cylindrical cavity that have a non-zero quadrupolar tensor. Several modes have $q_{ij} = 0$ due to symmetry.

C.2. optimal acoustic mode

As equation (15) suggests, the minimum detectable strain by the helium detector depends on several parameters. Thus, it is difficult to determine the best geometry for GW detection. In table C1, we analyze several acoustic modes for a cylindrical detector that have a non-zero quadrupole tensor. We have chosen each of these

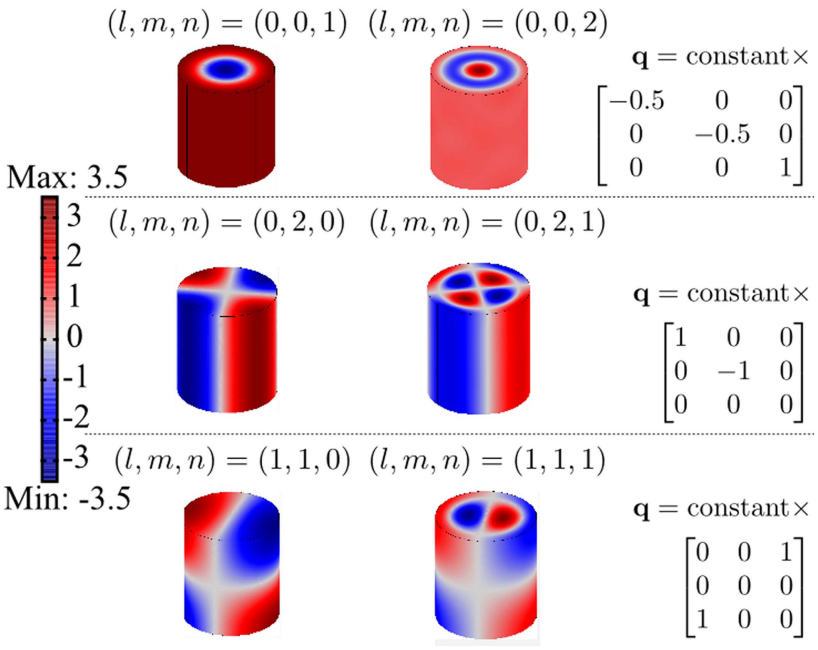

Figure C1. The first few pressure modes with non-zero quadrupolar tensors for the cylindrical cavity. While the form of quadrupolar tensor (shown on the right) is similar for many modes, the constant could be different for each acoustic mode.

Table C1. Table of modes and geometries of interest. We have chosen each of these geometries/modes to have a resonance frequency of 1075 $\pm$ 5 Hz, and assumed a Q-factor of 10^{11}. In particular, $h_{\rm min}$ is evaluated for pulsar J1843-1113. $\psi = \pi/2$, unless otherwise noted.

#	Mode	Dimensions	μ	A_G	Quadrupole tensor, q (kg m^2)	$d_{\rm max}$	$h_{\rm min}$ ($/\sqrt{\rm Hz}$)
1	[001]	$a = 0.135$ m, $L = 0.1$ m	$0.42M$	$0.14\pi r^2$	$0.028 \times \begin{bmatrix} -1/2 & 0 & 0 \\ 0 & -1/2 & 0 \\ 0 & 0 & 1 \end{bmatrix}$	1.875	1.69×10^{-22}
2	[001]	$a = 0.135$ m, $L = 0.3$ m	$0.42M$	$0.14\pi r^2$	$0.084 \times \begin{bmatrix} -1/2 & 0 & 0 \\ 0 & -1/2 & 0 \\ 0 & 0 & 1 \end{bmatrix}$	1.875	9.78×10^{-23}
3	[002]	$a = 0.245$ m, $L = 0.1$ m	$0.29M$	$0.01\pi r^2$	$0.01 \times \begin{bmatrix} -1/2 & 0 & 0 \\ 0 & -1/2 & 0 \\ 0 & 0 & 1 \end{bmatrix}$	1.875	5.99×10^{-22}
5	[020]	$a = 0.107$ m, $L = 0.1$ m	$0.51M$	$0.63\pi r^2$	$0.028 \times \begin{bmatrix} 1 & 0 & 0 \\ 0 & -1 & 0 \\ 0 & 0 & 0 \end{bmatrix}$	2.5 ($\psi = 0$)	1.10×10^{-22}
6	[021]	$a = 0.235$ m, $L = 0.1$ m	$0.34M$	$0.08\pi r^2$	$0.027 \times \begin{bmatrix} 1 & 0 & 0 \\ 0 & -1 & 0 \\ 0 & 0 & 0 \end{bmatrix}$	2.5 ($\psi = 0$)	2.05×10^{-22}
7	[110]	$a = 0.15$ m, $L = 0.123$ m	$0.14M$	$0.31\pi r^2$	$0.034 \times \begin{bmatrix} 0 & 0 & 1 \\ 0 & 0 & 0 \\ 1 & 0 & 0 \end{bmatrix}$	2.5	7.23×10^{-23}
8	[110]	$a = 0.45$ m, $L = 0.112$ m	$0.10M$	$0.26\pi r^2$	$-0.66 \times \begin{bmatrix} 0 & 0 & 1 \\ 0 & 0 & 0 \\ 1 & 0 & 0 \end{bmatrix}$	2.5	9.25×10^{-24}
9	[111]	$a = 0.22$ m, $L = 0.21$ m	$0.24M$	$0.04\pi r^2$	$-0.091 \times \begin{bmatrix} 0 & 0 & 1 \\ 0 & 0 & 0 \\ 1 & 0 & 0 \end{bmatrix}$	2.5	6.96×10^{-23}
10	[201]	$a = 0.3$ m, $L = 0.247$ m	$0.28M$	$0.04\pi r^2$	$-0.33 \times \begin{bmatrix} 1/2 & 0 & 0 \\ 0 & 1/2 & 0 \\ 0 & 0 & -1 \end{bmatrix}$	1.875	4.12×10^{-23}

geometries/modes to have a resonance frequency around 1075 Hz, and assumed a Q-factor of 10^{11}. In particular, $h_{\rm min}$ is evaluated for pulsar J1843-1113.

Before presenting a table analyzing 7 lower [*lmn*] modes of interest, we present a summary of some general trends:

(i) For the same mode and frequency, it is always advantageous to use a bigger mass (assuming *Q*-factor remains the same).

(ii) Higher *n* modes have significantly smaller effective area than lower *n* modes. This then contributes to lower strain sensitivity. Thus, it is advantageous to have the lowest *n* mode for a given frequency.

(iii) The maximum of the directivity function ($d^A(\theta, \phi)$) can vary by up to a factor of 4 in cylindrical geometry depending on the mode of interest.

Below we summarize various properties of ten different cylindrical geometries with similar resonance frequencies. Geometry 7 and 8 are used in the main text.

We find that for all $l = 0$ modes considered here, one needs a cylinder with length in meters to beat the 1 kHz sensitivity limit of advanced LIGO. The [020] mode has a particularly strong coupling to GWs due to its quadrupolar mode shape, and we choose this mode for the detector geometry discussed in the main text.

Due to its large effective area and directivity, the [110] mode also efficiently couples to gravitational metric strain. Unfortunately, the [110] mode does not couple to microwaves, so the GW signal in this acoustic mode cannot be detected using our proposed optomechanical technique. However, there might be other transduction schemes that enable efficient detection of this strain signal.

Finally, we would like to mention that while this paper deals exclusively with cylindrical geometry, there possibly are other geometries that couple more strongly to gravitational strain. Exploring different detector geometries is an interesting numerical problem that we hope to address in the future.

ORCID

I Pikovski https://orcid.org/0000-0002-9441-2553

References

[1] Abbott B P *et al* 2016 Observation of gravitational waves from a binary black hole merger *Phys. Rev. Lett.* **116** 061102
[2] Abbott B P *et al* 2016 Gw151226: observation of gravitational waves from a 22-solar-mass binary black hole coalescence *Phys. Rev. Lett.* **116** 241103
[3] Weisberg J M and Taylor J H 2004 The relativistic binary pulsar B1913+16: thirty years of observations and analysis *Conf. Proc. Binary Radio Pulsars* vol 328 *(Aspen, CO, 11–17 January)* ed F A Rasio and I H Stairs
[4] De Lorenzo L A and Schwab K C 2014 Superfluid optomechanics: coupling of a superfluid to a superconducting condensate *New J. Phys.* **16** 113020
[5] Weber J 1960 Detection and generation of gravitational waves *Phys. Rev.* **117** 306–13
[6] De Lorenzo L A and Schwab K C 2017 Ultra-high q acoustic resonance in superfluid ^{4}he *J. Low Temp. Phys.* **186** 233–40
[7] Schutz B F 1989 Gravitational wave sources and their detectability *Class. Quantum Grav.* **6** 1761
[8] Cutler C and Thorne K S 2002 An overview of gravitational-wave sources *Proc. GR16 Conf. General Relativity and Gravitation* ed N Bishop and S D Maharaj (Singapore: World Scientific) pp 72–111
[9] Riles K 2013 Gravitational waves: sources, detectors and searches *Prog. Part. Nucl. Phys.* **68** 1–54
[10] Abadie J *et al* 2010 Predictions for the rates of compact binary coalescences observable by ground-based gravitational-wave detectors *Class. Quantum Grav.* **27** 173001
[11] Vitale S 2014 Space-borne gravitational wave observatories *Gen. Relativ. Gravit.* **46** 1–19
[12] Shklovskii I S 1970 Possible causes of the secular increase in pulsar periods *Sov. Astron.* **13** 562–5
[13] Ostriker J P and Gunn J E 1969 On the nature of pulsars: I. Theory *Astrophys. J.* **157** 1395–417
[14] Ferrari A and Ruffini R 1969 Theoretical implications of the second time derivative of the period of the pulsar np 0532 *Astrophys. J.* **158** L71–5
[15] Melosh H J 1969 Estimate of the gravitational radiation from np 0532 *Nature* **224** 781–2
[16] Abbott B *et al* 2007 Upper limits on gravitational wave emission from 78 radio pulsars *Phys. Rev.* D **76** 042001
[17] Owen B J 2005 Maximum elastic deformations of compact stars with exotic equations of state *Phys. Rev. Lett.* **95** 211101
[18] Horowitz C J and Kadau K 2009 Breaking strain of neutron star crust and gravitational waves *Phys. Rev. Lett.* **102** 191102
[19] Pitkin M 2011 Prospects of observing continuous gravitational waves from known pulsars *Mon. Not. R. Astron. Soc.* **415** 1849–63
[20] Melatos A and Payne D J B 2005 Gravitational radiation from an accreting millisecond pulsar with a magnetically confined mountain *Astrophys. J.* **623** 1044–50
[21] Lyne A and Graham-Smith F 2006 *Pulsar Astronomy* (Cambridge: Cambridge University Press)
[22] Aasi J *et al* 2014 Gravitational waves from known pulsars: results from the initial detector era *Astrophys. J.* **785** 119
[23] Abdo A *et al* 2010 The first fermi large area telescope catalog of gamma-ray pulsars *Astrophys. J. Suppl. Ser.* **187** 460
[24] Abdo A *et al* 2013 The second fermi large area telescope catalog of gamma-ray pulsars *Astrophys. J. Suppl. Ser.* **208** 17
[25] Misner C W, Thorne K S and Wheeler J A 1973 *Gravitation* (San Francisco, CA: Freeman)
[26] Schutz B F 1984 Gravitational waves on the back of an envelope *Am. J. Phys.* **52** 412–9
[27] Carroll S M 2005 *Spacetime and Geometry. An Introduction to General Relativity* (Reading, MA: Addison-Wesley)
[28] Abbott B *et al* 2008 Beating the spin-down limit on gravitational wave emission from the crab pulsar *Astrophys. J. Lett.* **683** L45

[29] Lasky P D 2015 Gravitational waves from neutron stars: a review *Publ. Astron. Soc. Aust.* **32** e034
[30] Manchester R N, Hobbs G B, Teoh A and Hobbs M 2005 The australia telescope national facility pulsar catalogue *Astron. J.* **129** 1993–2006
[31] Palomba C 2000 Pulsars ellipticity revised *Astron. Astrophys.* **354** 163–8
[32] New K C B, Chanmugam G, Johnson W W and Tohline J E 1995 Millisecond pulsars: detectable sources of continuous gravitational waves? *Astrophys. J.* **450** 757
[33] Ushomirsky G, Cutler C and Bildsten L 2000 Deformations of accreting neutron star crusts and gravitational wave emission *Mon. Not. R. Astron. Soc.* **319** 902–32
[34] Abbott B P *et al* 2017 First search for gravitational waves from known pulsars with advanced ligo *Astrophys. J.* **839** 12
[35] Dupuis R J and Woan G 2005 Bayesian estimation of pulsar parameters from gravitational wave data *Phys. Rev.* D **72** 102002
[36] Abbott B P *et al* 2016 Gw150914: the advanced ligo detectors in the era of first discoveries *Phys. Rev. Lett.* **116** 131103
[37] Donnelly R J and Barenghi C F 1998 The observed properties of liquid helium at the saturated vapor pressure *J. Phys. Chem. Ref. Data* **27** 1217–74
[38] Landau L D and Lifshitz E M 1986 *Theory of Elasticity* (London: Butterworth-Heinemann)
[39] Kinsler L E, Fey A R, Coppens A B and Sanders J V 2000 *Fundamentals of Acoustics* (New York: Wiley)
[40] Hirakawa H 1976 Dispersion of gravitational waves *J. Phys. Soc. Japan* **35** 295–7
[41] Hirakawa H, Narihara K and Fujimoto M-K 1976 Theory of antennas for gravitational radiation *J. Phys. Soc. Japan* **41** 1093–101
[42] Bocko M F and Johnson W W 1984 Phase-sensitive parametric motion transducer *Phys. Rev.* A **30** 2135
[43] Aspelmeyer M, Meystre P and Schwab K 2012 Quantum optomechanics *Phys. Today* **65** 29–35
[44] Adhikari R X 2014 Gravitational radiation detection with laser interferometry *Rev. Mod. Phys.* **86** 121–51
[45] Fujii Y *et al* 2016 Active damping performance of the kagra seismic attenuation system prototype *J. Phys.: Conf. Ser.* **716** 012022
[46] Blair D G, Ju L and Peng H 1993 Vibration isolation for gravitational wave detection *Class. Quantum Grav.* **10** 2407
[47] Ivanov E N and Tobar M E 2006 Low phase-noise microwave oscillators with interferometric signal processing *IEEE Trans. Microw. Theory* **54** 3284–94
[48] Woode R A, Tobar M E, Ivanov E N and Blair D G 1996 An ultralow noise microwave oscillator based on a high-q liquid nitrogen cooled sapphire resonator *IEEE Trans. Ultrason. Ferroelectr. Freq. Control* **43** 936–41
[49] Bourhill J, Ivanov E and Tobar M E 2015 Precision measurement of a low-loss cylindrical dumbbell-shaped sapphire mechanical oscillator using radiation pressure *Phys. Rev.* A **92** 023817
[50] Blair D G, Ivanov E N, Tobar M E, Turner P J, van Kann F and Heng I S 1995 High sensitivity gravitational wave antenna with parametric transducer readout *Phys. Rev. Lett.* **74** 1908–11
[51] Allen M A, Farkas Z D, Hogg H A, Hoyt E W and Wilson P B 1971 Superconducting niobium cavity measurements at SLAC *IEEE Trans. Nucl. Sci.* **NS18** 168–72
[52] Eichhorn R, Gonnella D, Hoffstaetter G, Liepe M and Weingarten W 2014 On superconducting niobium accelerating cavities fired under N2-gas exposure arXiv:1407.3220
[53] Tobar M E and Blair D G 1993 Parametric transducers for resonant bar gravitational wave antennae *J. Phys. D: Appl. Phys.* **26** 2276
[54] Suh J *et al* 2014 Mechanically detecting and avoiding the quantum fluctuations of a microwave field *Science* **344** 1262–5
[55] Ivanov E N, Cuthbertson B D, Tobar M E and Blair D G 1996 Parametric back-action effects in a high-q cyrogenic sapphire transducer *Rev. Sci. Instrum.* **67** 2435
[56] Mitrofanov V P, Braginsky V B and Panov V I 1985 *Systems with Small Dissipation* (Chicago, IL: University of Chicago Press)
[57] Wollman E E *et al* 2015 Quantum squeezing of motion in a mechanical resonator *Science* **349** 952–5
[58] Pirkkalainen J-M, Damskägg E, Brandt M, Massel F and Sillanpää M A 2015 Squeezing of quantum noise of motion in a micromechanical resonator *Phys. Rev. Lett.* **115** 243601
[59] Lecocq F, Clark J B, Simmonds R W, Aumentado J and Teufel J D 2015 Quantum nondemolition measurement of a nonclassical state of a massive object *Phys. Rev.* X **5** 041037
[60] Tsubono K 1991 Detection of continuous waves *The Detection of Gravitational Waves* ed D G Blair (Cambridge: Cambridge University Press)
[61] Tobar M E and Blair D G 1993 Parametric transducers for resonant bar gravitational wave antennae *J. Phys. D: Appl. Phys.* **26** 2276
[62] Tobar M E, Ivanov E N and Blair D G 2000 Parametric transducers for the advanced cryogenic resonant-mass gravitational wave detectors *Gen. Relativ. Gravit.* **32** 1799–821
[63] Ju L, Blair D G and Zhao C 2000 Detection of gravitational waves *Rep. Prog. Phys.* **63** 1317
[64] Armano M *et al* 2016 Sub-femto-g free fall for space-based gravitational wave observatories: Lisa pathfinder results *Phys. Rev. Lett.* **116** 231101
[65] Hogan J M *et al* 2011 An atomic gravitational wave interferometric sensor in low earth orbit (agis-leo) *Gen. Relativ. Gravit.* **43** 1953
[66] Hobbs G *et al* 2010 The international pulsar timing array project: using pulsars as a gravitational wave detector *Class. Quantum Grav.* **27** 084013
[67] Rojas X and Davis J P 2015 Superfluid nanomechanical resonator for quantum nanofluidics *Phys. Rev.* B **91** 024503
[68] Arvanitaki A and Geraci A A 2013 Detecting high-frequency gravitational waves with optically levitated sensors *Phys. Rev. Lett.* **110** 071105
[69] Goryachev M and Tobar M E 2014 Gravitational wave detection with high frequency phonon trapping acoustic cavities *Phys. Rev.* D **90** 102005
[70] Bonazzola S and Gourgoulhon E 1996 Gravitational waves from pulsars: emission by the magnetic-field-induced distortion *Astron. Astrophys.* **312** 675–90
[71] Christensen N 1992 Measuring the stochastic gravitational-radiation background with laser-interferometric antennas *Phys. Rev.* D **46** 5250–66
[72] Creighton J D E and Anderson W G 2011 *Gravitational-Wave Physics and Astronomy: An Introduction to Theory, Experiment and Data Analysis* (New York: Wiley)
[73] Cognard I and Backer D C 2004 A microglitch in the millisecond pulsar PSR B1821-24 in M28 *Astrophys. J.* **612** L125–7
[74] Haskell B 2008 Mountains on neutron stars *Class. Quantum Grav.* **25** 114049
[75] Vigelius M and Melatos A 2009 Improved estimate of the detectability of gravitational radiation from a magnetically confined mountain on an accreting neutron star *Mon. Not. R. Astron. Soc.* **395** 1972–84